blood®
Regular Article

IMMUNOBIOLOGY AND IMMUNOTHERAPY

Dominant activating RAC2 mutation with lymphopenia, immunodeficiency, and cytoskeletal defects

Amy P. Hsu,[1] Agnes Donkó,[2,*] Megan E. Arrington,[3,*] Muthulekha Swamydas,[4,*] Danielle Fink,[5,*] Arundhoti Das,[6] Omar Escobedo,[2] Vincent Bonagura,[7] Paul Szabolcs,[8] Harry N. Steinberg,[9] Jenna Bergerson,[1] Amanda Skoskiewicz,[10] Melanie Makhija,[10] Joie Davis,[1] Ladan Foruraghi,[1] Cindy Palmer,[1] Ramsay L. Fuleihan,[10] Joseph A. Church,[11,12] Avinash Bhandoola,[6] Michail S. Lionakis,[4] Sharon Campbell,[13] Thomas L. Leto,[2] Douglas B. Kuhns,[5] and Steven M. Holland[1]

[1]Immunopathogenesis Section and [2]Molecular Defenses Section, Laboratory of Clinical Immunology and Microbiology (LCIM), National Institute of Allergy and Infectious Diseases (NIAID), National Institutes of Health (NIH), Bethesda, MD; [3]Chemistry, University of North Carolina (UNC), Chapel Hill, NC; [4]Fungal Pathogenesis Section, LCIM, NIAID, NIH, Bethesda, MD; [5]Neutrophil Monitoring Laboratory, Leidos Biomedical Research, Inc., Frederick National Laboratory for Cancer Research, Frederick, MD; [6]Laboratory of Genome Integrity, Center for Cancer Research, National Cancer Institute, NIH, Bethesda, MD; [7]Cohen Children's Medical Center, New York, NY; [8]UPMC Children's Hospital of Pittsburgh, Pittsburgh, PA; [9]North Shore University Hospital, New Hyde Park, NY; [10]Ann & Robert H. Lurie Children's Hospital of Chicago, Chicago, IL; [11]Pediatric Allergy/Immunology, Children's Hospital Los Angeles, Los Angeles, CA; [12]Clinical Pediatrics, Keck School of Medicine of USC, Los Angeles, CA; and [13]Biochemistry and Biophysics, UNC Lineberger Comprehensive Cancer Center, UNC, Chapel Hill, NC

KEY POINTS

- **E62K is a dominant activating mutation of the small GTPase, RAC2; patients with RAC2[E62K] have lymphoid and myeloid defects.**
- **Rac2$^{+/E62K}$ mice phenocopy the T- and B-cell lymphopenia, increased neutrophil F-actin, and excessive superoxide production seen in patients.**

Ras-related C3 botulinum toxin substrate 2 (RAC2), through interactions with reduced NAD phosphate oxidase component p67^{phox}, activates neutrophil superoxide production, whereas interactions with p21-activated kinase are necessary for fMLF-induced actin remodeling. We identified 3 patients with de novo RAC2[E62K] mutations resulting in severe T- and B-cell lymphopenia, myeloid dysfunction, and recurrent respiratory infections. Neutrophils from RAC2[E62K] patients exhibited excessive superoxide production, impaired fMLF-directed chemotaxis, and abnormal macropinocytosis. Cell lines transfected with RAC2[E62K] displayed characteristics of active guanosine triphosphate (GTP)–bound RAC2 including enhanced superoxide production and increased membrane ruffling. Biochemical studies demonstrated that RAC2[E62K] retains intrinsic GTP hydrolysis; however, GTPase-activating protein failed to accelerate hydrolysis resulting in prolonged active GTP-bound RAC2. Rac2$^{+/E62K}$ mice phenocopy the T- and B-cell lymphopenia, increased neutrophil F-actin, and excessive superoxide production seen in patients. This gain-of-function mutation highlights a specific, nonredundant role for RAC2 in hematopoietic cells that discriminates RAC2 from the related, ubiquitous RAC1. (*Blood*. 2019;133(18):1977-1988)

Introduction

Ras-related C3 botulinum toxin substrate 2 (RAC2) is a small guanine nucleotide-binding protein in the Rho subclass of RAS superfamily GTPases encoded by *RAC2* and expressed primarily in hematopoietic cell lineages. Functionally, it was first identified as the GTPase involved in reduced NAD phosphate (NADPH) oxidase activation[1] as well as actin cytoskeleton remodeling.[2] Additionally, RAC2 is involved in membrane ruffling,[3] Fcγ receptor-mediated phagocytosis, and phagocytic cup and macropinosome formation.[4] The RAC2 dominant loss-of-function mutation, p.D57N, has been reported in 2 infants, 1 with severe phagocyte immune deficiency[5] and the other with absent T-cell receptor excision circles (TRECs) detected by newborn screening.[6] Both patients had severe phagocyte defects, including defective superoxide $O_2^{\cdot-}$ formation and adhesion, proving essential roles for RAC2 in those processes. More recently, a pair of consanguineous siblings was described with homozygous null RAC2 alleles (p.W56X), who had lymphopenia and recurrent sinopulmonary infections, clinically diagnosed as common variable immunodeficiency.[7] Last, both Rac2$^{-/-}$ and Rac2$^{+/-}$ mice exhibit decreased neutrophil chemotaxis with decreased F-actin[8] and NADPH oxidase formation in response to fMLF.[9]

The nucleotide-bound state of RAC GTPases is tightly regulated, determining the activation state of RAC. Activation generally requires release of inactive, guanosine diphosphate (GDP)–bound RAC2 from a guanine nucleotide dissociation inhibitor (GDI), RhoGDI, followed by association with a guanine exchange factor (GEF), such as TIAM1.[10] This activation occurs only after an appropriate stimulus such as the chemoattractant, fMLF. The RAC2/GEF interaction releases GDP, allowing binding of guanosine triphosphate (GTP) and resulting in active RAC2. RAC2-GTP drives diverse cellular functions through association and activation of downstream effector proteins including p67^{phox}[11] and PAK1.[12] Activation of these downstream targets leads to $O_2^{\cdot-}$ production,[1]

actin cytoskeleton rearrangement,[2] thymic T-cell selection,[13] and p38 kinase activation.[3] GTPase-activating proteins (GAPs) such as p50RhoGAP[14] associate with RAC2-GTP to stimulate GTP hydrolysis, resulting in the inactive RAC2-GDP, which again associates with RhoGDI.

Primary immune deficiencies (PIDs) often underlie opportunistic infections or aberrant responses to infection. Next-generation sequencing applied to PID patients has identified important mutations, even in adults. Identification and characterization of a gain-of-function RAC2 mutation in PID patients demonstrated a critical requirement of RAC2 cycling between inactive GDP and active GTP bound states to regulate $O_2^{\cdot}$ production, lymphocyte development, and actin cytoskeletal remodeling.

Methods

Study patients

Study participants or their parents provided written informed consent to participate in an institutional review board–approved protocol at the National Institute of Allergy and Infectious Diseases (NIAID), National Institutes of Health.

Rac2$^{+/E62K}$ Mice

Mice were maintained under specific pathogen-free housing conditions at an American Association for the Accreditation of Laboratory Animal Care–accredited animal facility at NIAID, housed in accordance with procedures outlined in Guide for the Care and Use of Laboratory Animals under a NIAID Animal Care and Use Committee–approved protocol. Three- to 4-week old superovulated C57BL/6 mice were used as embryo donors and were mated with C57BL/6 males. Fertilized embryos were collected from the oviducts and microinjected with a mixture of Cas9 (10 ng/μL), single guide RNA (10 ng/μL), and 121b ss-oligo nucleotide (20 ng/μL). Microinjected embryos were transferred into oviducts of CD1 pseudo-pregnant mothers, resulting pups were weaned at 3 weeks; ear punch biopsies were used for genotyping.

Sequencing

Genomic DNA from peripheral blood leukocytes or ear punch biopsies was amplified using gene-specific primers and sequenced using Big Dye Terminators v3.1. Resulting chromatograms were compared with National Center for Biotechnology Information reference sequences, NM_002872.4, human; NM_009008.3, mouse) using Sequencher.

Cell culture and transfections

pcDNA3.1 expression vectors for RAC2 wild-type (WT) or RAC2 [E62K], gp91^{phox}/NOX2, p67^{phox}, p47^{phox}, and GFP were transfected into COS-7 or Raw264.7 cells using Lipofectamine-3000 or Lipofectamine-LTX-Plus (Thermo Fisher Scientific), respectively.

Reactive oxygen species assay

Cells, with or without phorbol 12-myristate 13-acetate (PMA) stimulation, were harvested 48 hours posttransfection. Cell suspension diluted with Diogenes reagent was measured at 1-minute intervals for 30 minutes on a Luminoskan Ascent plate reader (Thermo Fisher Scientific).

Immunostaining and confocal microscopy

After 48 hours of expression, cells in glass-bottom dishes were washed, fixed with 4% paraformaldehyde, permeabilized with 0.3% Triton X-100, and stained for F-actin and RAC2. Cells were counterstained with 4′,6-diamidino-2-phenylindole nuclear marker and mounted with Prolong antifade.

RAC2 PBD-binding assays and western blot

Glutathione *S*-transferase (GST)-PAK1 p21 binding domain (residues 70-117) fusion protein (Addgene, deposited by Jonathan Chernoff) was isolated from transformed *Escherichia coli* using glutathione-sepharose beads.[15] COS-7 cells transfected with RAC2-WT or RAC2[E62K] were lysed; lysates were cleared by centrifugation. Supernatants were incubated with purified GST-p21 protein binding domain (PBD) linked to glutathione-agarose beads. A total of 25 μg protein lysates or 25 μL of eluted precipitates were used for western blot analysis of GST-PBD–bound RAC2. Western blot analysis was performed by standard protocols using RAC2 (Millipore), AKT, phosphorylated AKT (pAKT), and glyceraldehyde-3-phosphate dehydrogenase (Cell Signaling) primary antibodies and HRP-conjugated (Sigma Aldrich) secondary antibodies.

Neutrophil analysis

Neutrophils were isolated from heparinized blood by standard procedures. F-actin staining–polymorphonuclear leukocyte (PMNs; 1×10^6) were incubated with 37% formaldehyde, 5 U/mL phalloidin, and 1 mg/mL dry lysophosphatidylcholine, and washed and analyzed on BD Canto II flow cytometer.

Chemotaxis–isolated PMNs (5×10^3 cells) and fMLF were added to appropriate wells of an EZ-TAXIScan instrument. Digital images were acquired every 30 seconds for 1 hour. Images were converted to stacks using ImageJ software (version 1.46r, National Institutes of Health), MTrackJ plug-in was used to track individual cell migration, and track measurements were analyzed using Microsoft Excel.

Macropinocytosis PMNs were incubated with AlexaFluor-488–labeled Dextran (Molecular Probes) for 10 minutes. Cells were washed, fixed, placed on slides, and air dried.

Extracellular $O_2^{\cdot}$ production by cytochrome c reduction

PMNs (0.25×10^6/mL) were incubated with 100 mM cytochrome c for 15 minutes after addition of either buffer, PMA (100 ng/mL), or fMLF (10^{-7} M). The supernatant was analyzed spectrophotometrically for $O_2^{\cdot}$ -dependent reduction of cytochrome c. For kinetic study, basal or stimulated $O_2^{\cdot}$ production was monitored every 15 seconds for 30 minutes.

Purification of recombinant proteins

Plasmids containing the catalytic GAP domain of p50RhoGAP (amino acids 244-431) and PAK-PBD were gifts from Keith Burridge, University of North Carolina, Chapel Hill); catalytic GEF domain of TIAM1 (amino acids 1033-1406 was a gift from Sondek Laboratory, University of North Carolina, Chapel Hill). Full-length RAC2-WT (Origene) was mutated to create RAC2 [E62K]. Plasmids were transformed into *E coli* cells, protein expression induced overnight, and proteins isolated as

previously described.[16] GDP exchange and GTP hydrolysis assays were performed as previously described.[17]

Flow cytometric analysis of mouse peripheral blood

Single-cell suspensions of peripheral blood were obtained as previously described.[18] Cells were stained with 1:500 dilution of live/dead dye for 10 minutes, blocked with rat anti-mouse CD16/32 and 0.5% bovine serum antigen, and then surface stained using fluorescently conjugated antibodies against mouse CD45 (30-F11), CD19 (1D3), NK1.1 (PK136) (eBioscience), CD3e (145-2C11; BD Biosciences), CD4 (GK1.5), and CD8 (53-6.7) (BioLegend). Cells were collected on an LSR II Fortessa and data were analyzed using FlowJo. Cell numbers were quantified using phycoerythrin-conjugated fluorescent counting beads.

Isolation of murine neutrophils from bone marrow

Neutrophils were isolated from mouse bone marrow using Histopaque gradient separation as described.[19]

Results

Study patients

Patient 1 presented to the National Institutes of Health Clinical Center at age 37 for recurrent pulmonary infections. Since the age of 2 years, she had pancytopenia, recurrent sinusitis, and pneumonia, including 1 episode of *Neisseria meningitidis* type Y pneumonia and sepsis, lymphadenitis, varicella zoster infection, urinary tract infections, and cellulitis. (Cell counts, proliferation studies, and immunoglobulins are outlined in Table 1.) Splenectomy at 22 years for pancytopenia showed littoral cell angioma. Neutrophil and platelet counts improved postsplenectomy, but recurrent infections required multiple hospitalizations and intravenous antibiotics despite immunoglobulin replacement. Bronchiectasis was complicated by *Aspergillus* spp., *Staphylococcus aureus, Mycobacterium abscessus*, and *Mycobacterium avium* complex. Whole exome sequencing identified a novel, heterozygous variant in *RAC2*, c.184G>A, p.E62K (Figure 1A). The equivalent representation of mutant and WT reads and sufficient read depth (98) plus absence of the variant in both parents suggest a de novo mutation. A matched unrelated donor hematopoietic stem cell transplant at age 42 years led to full immune reconstitution and improved lung function.

Patient 2 was identified with low TRECs (13/μL; normal value >22/μL) and reduced peripheral $CD3^+$ T-cell counts on newborn screening (Table 1). She had normal proliferation to both phytohemagglutinin and pokeweed mitogen at 3 weeks and 8 months. A targeted immunodeficiency gene panel (Invitae Primary Immunodeficiency Panel) identified de novo heterozygous *RAC2* c.184G>A, p.E62K. By age 9 months, she had acute bronchitis with persistent wheezing. At 1 year, she remained lymphopenic (CD3, <100 cells), leading to successful hematopoietic stem cell transplantation at age 2 from a matched sibling donor.

Patient 3 was referred at age 14 years for lymphopenia, recurrent herpes stomatitis, and recurrent otitis media. He had a vesicular eruption with fever after varicella vaccination and developed shingles at age 3. He had chronic rhinitis and cough with negative testing to environmental allergens, normal to elevated serum immunoglobulin G (IgG), low IgM, and normal IgA, with marked diminution in all lymphocyte subsets (Table 1). Antibodies to tetanus, varicella, and a few pneumococcal serotypes were adequate with poor response to *Haemophilus influenzae* type b. Targeted in-house immunodeficiency gene panel at Lurie Children's Hospital identified de novo heterozygous *RAC2* c.184G>A, p.E62K.

Identification of *RAC2* mutation

Whole exome sequencing was performed on patient 1. Coding variants not present in the Single Nucleotide Polymorphism Database (dbSNP), version 135, were filtered against the International Union of Immunologic Societies (IUIS) gene list. Only *RAC2* was associated with a dominant phenotype, and functional testing was pursued. The novel, heterozygous variant in *RAC2*, c.184G>A, p.E62K, was Sanger confirmed in all cases. This variant is not present in the Genome Aggregation Database (gnomAD), nor has it been seen in any other patient in our cohort.

Glutamate 62 (E62) lies within the Switch II domain of RAC2 (Figure 1B) and is highly conserved across the RAC and RAS GTPases.[20] Additional reported Switch II variants are noted by asterisks within the protein alignment, including somatic mutations at RAC1[Q61][21] and RAC2[D63][22] as well as the recently described germline CDC42[Y64C].[23] The crystal structure of the closely related RAC1 is shown in Figure 1C, with the Switch II domain highlighted in blue, the previously reported RAC2[D57N] in magenta, and RAC2[E62K] in red.

RAC2[E62K] patient neutrophils have aberrant macropinocytotic vesicles

Abnormal neutrophils were apparent in all 3 patients by light microscopy. Large vacuoles were present in many of the neutrophils (Figure 2A) as well as some lymphocytes (data not shown). These vacuoles were clearly seen by transmission electron microscopy (Figure 2B) and were absent in healthy controls. Strikingly, patient 3 had "toxic vacuolation" on a manual complete blood count. His cells (supplemental Figure 1A, available on the *Blood* Web site) showed enlarged macropinocytotic vesicles in lymphocytes as well as neutrophils.

Recognizing that RAC molecules are involved in phagosome[4] and macropinosome[24] formation, and that RAC2[D57N] mutation inhibited macropinocytosis,[3] we hypothesized the large neutrophil vacuoles were macropinosomes. Neutrophils from healthy controls, patient 2, (Figure 2C) and patient 3 were incubated with fluorescein isothiocyanate (FITC)-dextran to measure fluid endocytosis by macropinocytosis. Measuring individual cell fluorescence and correcting for background, cells from patients contained significantly more FITC-dextran than those from healthy controls (Figure 2D; supplemental Figure 1B). Further, it appears the FITC is contained in well-defined compartments similar to the vacuoles seen by light microscopy.

RAC2[E62K] results in enhanced neutrophil $O_2^{\cdot-}$ production

RAC2 is the small GTPase associated with the NADPH oxidase complex in hematopoietic cells.[1] Neutrophils from *Rac2*$^{-/-}$ mice exhibited impaired $O_2^{\cdot-}$ production in response to both PMA and fMLF,[8] whereas RAC2[D57N] patients do so only in response to fMLF.[5,6] To assess cytochrome c reduction by $O_2^{\cdot-}$ in RAC2[E62K] patient neutrophils, we evaluated temporal $O_2^{\cdot-}$ release

Table 1. Immunologic findings

	Patient 1		Patient 2			Patient 3	
Age	37 y	38 y	2 wk	8 mo	17 mo	4 y	14 y
$CD3^+$	79 (708-2227)	209 (714-2266)	295 (2500-5500)	235	128	193 (1051-3031)	137
$CD3^+CD4^+$	36 (479-1445)	124 (359-1565)	270 (1600-4000)	192	103	84 (548-1720)	47
$CD3^+CD8^+$	20 (225-753)	81 (178-853)	20 (560-1700)	21	16	113 (332-1307)	90
$CD19^+$	8 (68-444)	13 (59-329)	115 (300-2000)	160	117	80 (203-1139)	33
$CD3^-CD16^+CD56^+$	7 (48-474)	9 (126-729)	50 (170-1100)	52	27	87 (138-1027)	75
Mitogen proliferation (PHA)	Normal	ND	ND	Normal	Normal	Normal (10 y)	ND
Antigen proliferation (Candida)	Absent	ND	ND	Absent		SI, 1.3 (>18)*	ND
TREC	ND	ND	13 (>22)	ND	ND	ND	ND
Serum IgG, mg/dL	ND		176 (231-1411)	405		1400 (572-1474) (7 y)	1110 (716-1711)
Serum IgA, mg/dL	ND	75 (91-499)	ND	60 (16-83)	58 (14-105)	43.1 (69-309) (7 y)	53.6 (68-378)
Serum IgM, mg/dL	ND	14 (34-342)	ND	26 (0-145)	67 (19-146)	19.5 (53-334) (7 y)	11.9

$CD3^+$ T cells, with $CD4^+$ and $CD8^+$ subsets, $CD19^+$ B cells, and $CD3^-CD16^+CD56^+$ NK cells were measured in the patients at the ages indicated. Counts per milliliter of blood are listed as well as the normal reference range for the testing laboratory. Where available, results for mitogen and antigen proliferation, T-cell receptor excision circle measurements, and immunoglobulin levels are included.

ND, not tested; PHA, phytohemagglutinin; SI, stimulation index.

*SI was low; however, basal proliferation was high, skewing interpretation of results.

and accumulation in the supernatant. Similar to the RAC2[D57N] patients, RAC2[E62K] patient neutrophils responded normally to PMA (data not shown). After stimulation with fMLF, control neutrophils produced increasing amounts of $O_2^{\bullet}$ until, by 4 minutes, production ceased, and the detected $O_2^{\bullet}$ remained relatively constant. In contrast, patient neutrophils produced $O_2^{\bullet}$ with an increased rate and duration (Figure 2E). The cumulative $O_2^{\bullet}$ production from patient neutrophils was three- to fourfold greater than healthy controls (Figure 2F).

RAC2[E62K] neutrophils have abnormal chemotaxis

Because neutrophils from both *Rac2*$^{-/-}$ mice and the previously reported RAC2[D57N] patients had impaired chemotaxis in response to fMLF,[6,25,26] we evaluated fMLF-directed chemotaxis in patient neutrophils. Time-lapse video of cells from patient 1 (supplemental Video 1) demonstrated drastically impaired chemotactic velocity toward fMLF compared with healthy control cells (supplemental Video 2). Individual cell tracking from patients 1 and 2 showed both fewer patient cells moving and decreased distance traveled per cell (Figure 2G; supplemental Figure 1C). Control cells completed chemotaxis across the chamber within 30 to 40 minutes, whereas few patient cells had migrated halfway across the chamber after 60 minutes (Figure 2H). Interestingly, patients 2 and 3 reported normal Boyden chamber chemotaxis assays before National Institutes of Health referral, highlighting the importance of direct tracking of individual cells in this chemotactic defect.

RAC2 is involved in the cycling of actin between monomeric (G-actin) and filamentous (F-actin) states through interactions with both cofilin and the ARP2/3 complex.[27] Neutrophils from patient 1 (supplemental Figure 1D) exhibited an increased F-actin content. Considering actin remodeling as a dynamic process, we compared neutrophil F-actin following fMLF stimulation between controls and patient 3. Although control neutrophils had a transient increase in F-actin, peaking between 10 and 15 seconds followed by rapid decline, cells from patient 3 peaked at 30 seconds and maintained high levels of F-actin even at 60 seconds (supplemental Figure 1E). These data suggest impaired actin cycling, which may explain their chemotactic defect.

Transfected cells recapitulate the RAC2[E62K] cellular phenotype

Three unrelated patients with the same de novo mutation in *RAC2* strongly suggested genetic causality. To prove RAC2 [E62K] was responsible for the patient cellular features, COS7 cells were cotransfected with expression constructs for members of the NADPH oxidase and either RAC2[WT], RAC2[E62K], or GFP. Reactive oxygen species (ROS) production over time was measured under basal and PMA-stimulated conditions. RAC2 [WT] cells showed minimal basal ROS production that increased after PMA addition (Figure 3A, top). In contrast, RAC2[E62K]-transfected cells showed elevated basal ROS production with significant augmentation after PMA (Figure 3A, middle); cells transfected with GFP alone did not produce ROS (Figure 3A, bottom). These data were quantified using integrated 30-minute chemiluminescence (Figure 3B) and are consistent with the increased ROS production observed in patient neutrophils.

RAC2-GTP interacts with PAK1 PBD to mediate the actin cytoskeletal rearrangement that occurs during phagocytosis.[4]

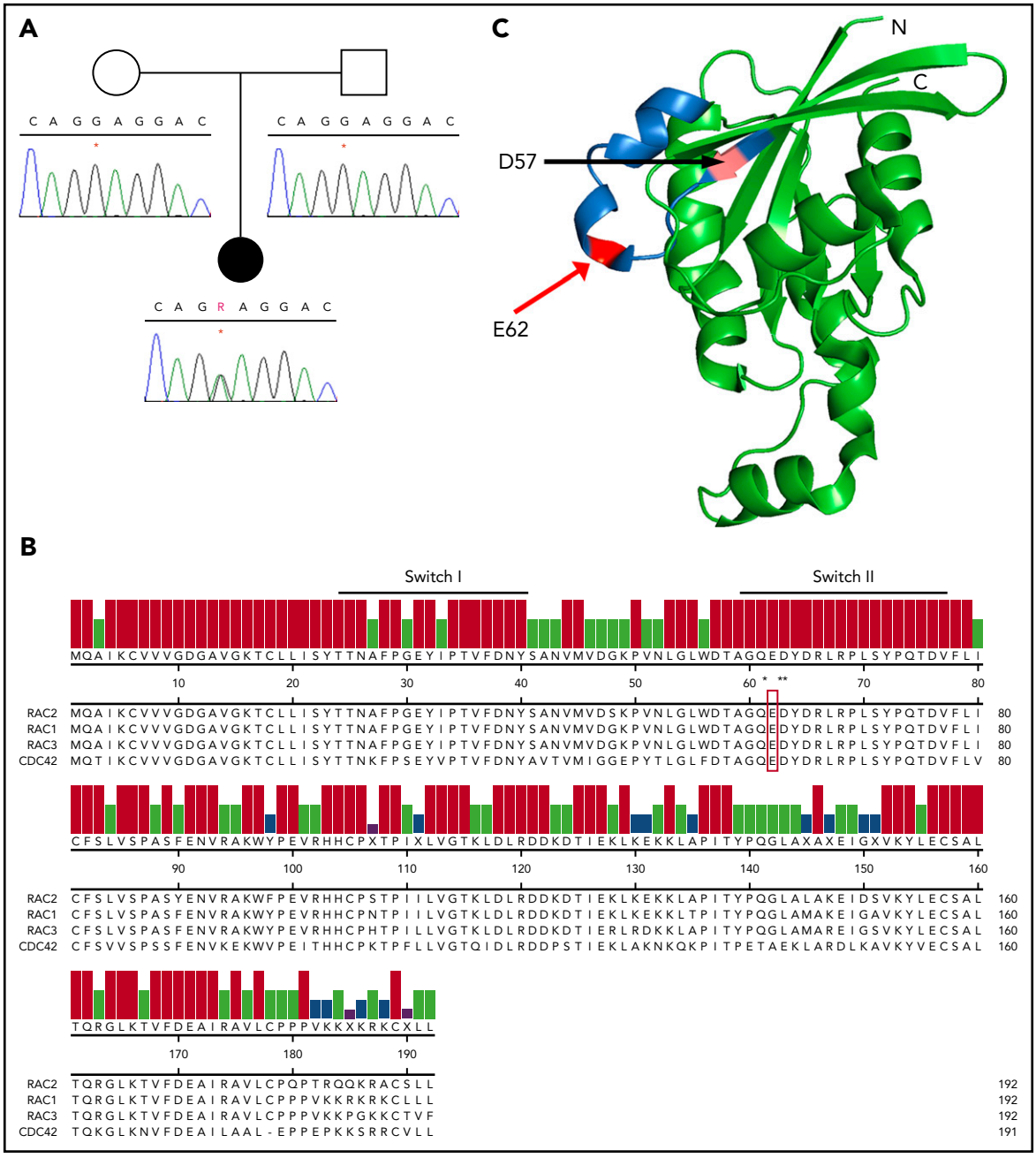

Figure 1. RAC2 mutation occurs within the highly conserved Switch II domain. (A) Sanger sequence of *RAC2* exon 3 demonstrating c.184G>A in patient 1 (*) and wild-type sequence in both parents. (B) Amino acid alignment of select members of human RHO family of GTPases. Reference sequences (RAC2 NP_002863.1, RAC1 NP_008839.2, RAC3 NP_005043.1, CDC42 NP_001782.1) are from the National Center for Biotechnology Information and aligned using Clustal W. Underline, conserved Switch I and Switch II regions; open box, E62; *Q61, D63, and Y64. (C) Three-dimensional structure of the related RAC1 (3TH5)[46]; blue, Switch II; pink, D57 residue; and red, E62. C, C terminus; N, N terminus.

Given the abnormal chemotaxis, altered F-actin staining, and increased macropinocytosis in patient neutrophils, we hypothesized that RAC2-PAK1 interactions were increased. Using lysates from transfected cells, we precipitated proteins that bound the purified GST fusion protein of the PAK1-PBD immobilized on glutathione-agarose and probed the resulting blot for RAC2. Quantifying the immunoblot by densitometry and normalizing for RAC2 content showed increased levels of PAK1-PBD–associated RAC2 in the E62K-transfected cells compared with WT (Figure 3C), suggesting more RAC2[E62K] is in its active GTP-bound form than RAC2[WT].

Active, GTP-bound RAC2 interacts with PAK1, resulting in the PAK1-C-terminal domain becoming a scaffold for AKT and leading to membrane translocation and phosphorylation of AKT (pAKT).[28] Expression of the dominant-negative Rac^{N17} inhibited PAK1-induced pAKT, whereas expression of the constitutively active Rac^{V12} increased association of AKT with PAK1.[28] We examined the effect of RAC2[E62K] on AKT using lysates from transfected COS-7 cells by immunoblot and quantified the total AKT and pAKT levels using densitometry. After normalizing for total AKT levels, cells transfected with RAC2[E62K] showed increased pAKT compared with RAC2[WT] (Figure 3D).

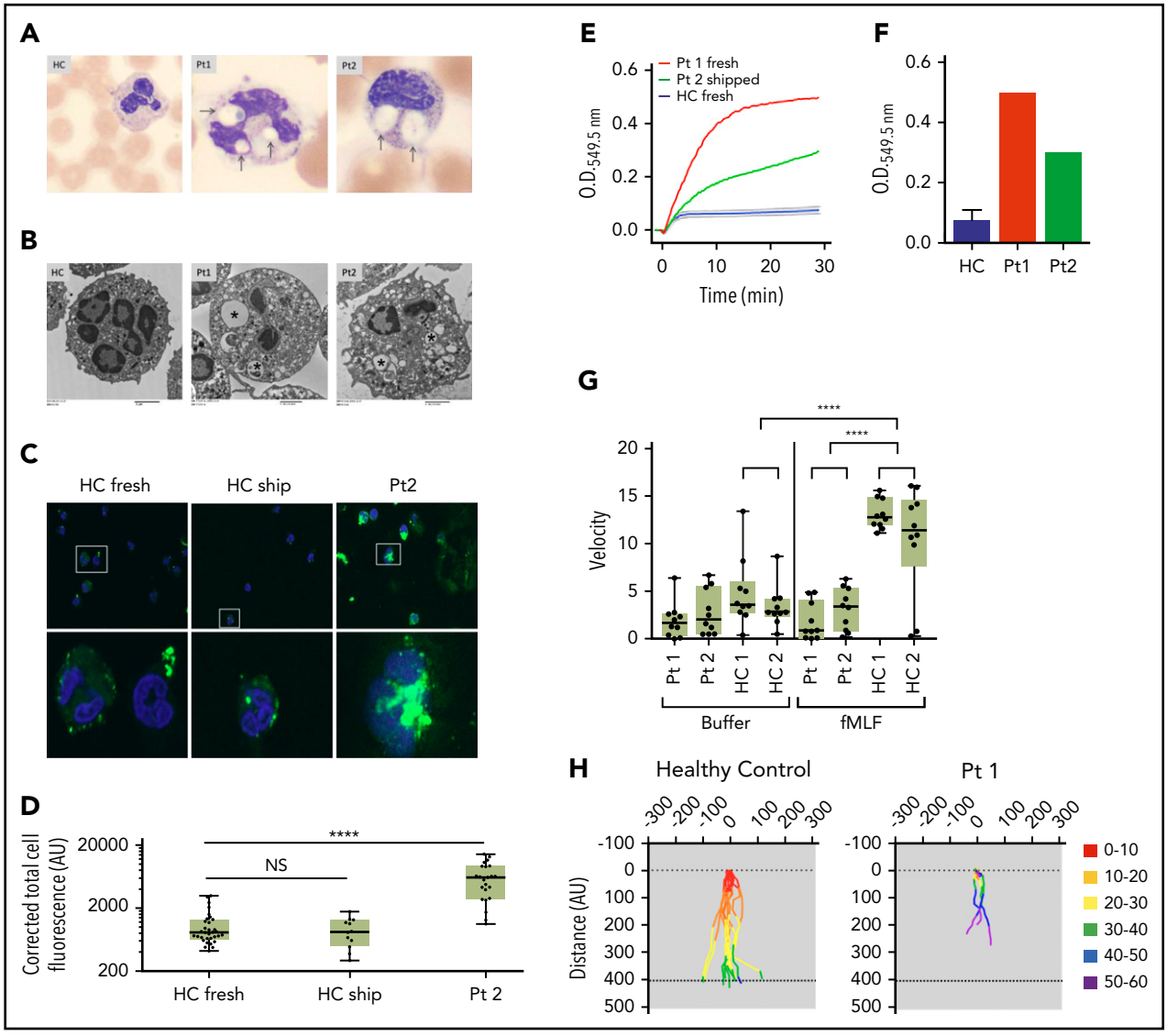

Figure 2. Neutrophils from patients have large macropinocytotic vesicles, excess superoxide production and diminished fMLF-induced chemotaxis. (A) Light microscopy images of blood smears from health control (HC), patient (Pt)1, and Pt2. Large vacuoles are clearly present within the neutrophils of Pt1 and Pt2 (arrows). Images acquired from a CellaVision DM1200. Original magnification ×100. (B) Transmission electron microscopy of neutrophils from HC, Pt1, and Pt2. *Large vacuoles are seen in both patients. Paucity of specific granules in Pt1 compared with HC. Images were acquired using a Hitachi H7600 transmission electron microscope and an AMT XR41B digital camera. Original magnification of HC and Pt2, ×3000; original magnification of Pt1, ×2500. (C) Neutrophils from HC either fresh (left) or shipped along with the patient sample (middle) and Pt2 (right) were incubated with FITC-dextran for 15 minutes. Cells were fixed and viewed using Images and were acquired using EVOS FL system with ×40 and ×100 magnification and analyzed with ImageJ software to determine the cell area, integrated density, and mean. Corrected total cell fluorescence = integrated density – (area × mean of background readings). (D) Total fluorescence of FITC-dextran cells corrected for background fluorescence. Calculations from 10 to 30 individual cells from each sample were plotted. *P* values were calculated using 1-way ANOVA correcting for multiple comparisons. ****$P <$ .0001. (E) Neutrophil extracellular superoxide production kinetics measured every 15 seconds after fMLF treatment of cells from Pt1 (red) and Pt2 (green) compared with 6 HCs (blue line with error bars) showing superoxide production over 30 minutes, evaluated every 15 seconds. (F) Cumulative superoxide production after 30 minutes. (G) Net chemotactic velocity of 10 individual cells from patients 1 and 2 compared with 2 HC with buffer alone (left) or fMLF (right). Two-way analysis of variance (ANOVA) correcting for multiple comparisons was used for calculating significance. ****$P <$ .0001. (H) Individual cell tracings from Pt1 (right) and HC (left) tracking movement and colored by 10-minute increments. AU, arbitrary unit; O.D., optical density.

The increased PAK1 binding and pAKT seen in RAC2[E62K]-transfected cells are associated with membrane ruffling and macropinosome formation. Using confocal microscopy, we explored the effects of transfection of RAC2[WT] or RAC2[E62K] on RAW264.7 or COS-7 cells. RAC2[E62K]-transfected RAW264.7 cells showed increased membrane ruffling (Figure 3E, top; supplemental Figure 2, top 2 rows), a precursor to macropinocytosis and driven by RAC2-PAK1-pAKT interaction near the cell membrane. Distinctively, the RAC2[E62K]-transfected COS-7 cells exhibited large vesicles (Figure 3F, bottom; supplemental Figure 2, bottom 2 rows) similar to the macropinosomes seen in patient neutrophils.

Cognate GEF and GAP proteins fail to regulate RAC2[E62K]

E62 is a conserved residue within the Switch II domain found in all Rho GTPases; previous work on RAS and RhoA demonstrated that mutation to either alanine or lysine resulted in disruption of GEF-mediated guanine nucleotide exchange.[20] Isolated GTPases have a slow intrinsic rate of nucleotide exchange, significantly increased by GEF binding. We compared intrinsic and TIAM1-associated GDP dissociation rates using RAC2 preloaded with ^{mant}GDP, which fluoresces when bound to RAC2. Exchange of ^{mant}GDP for unlabeled GDP causes decreased fluorescence measured over time. Both

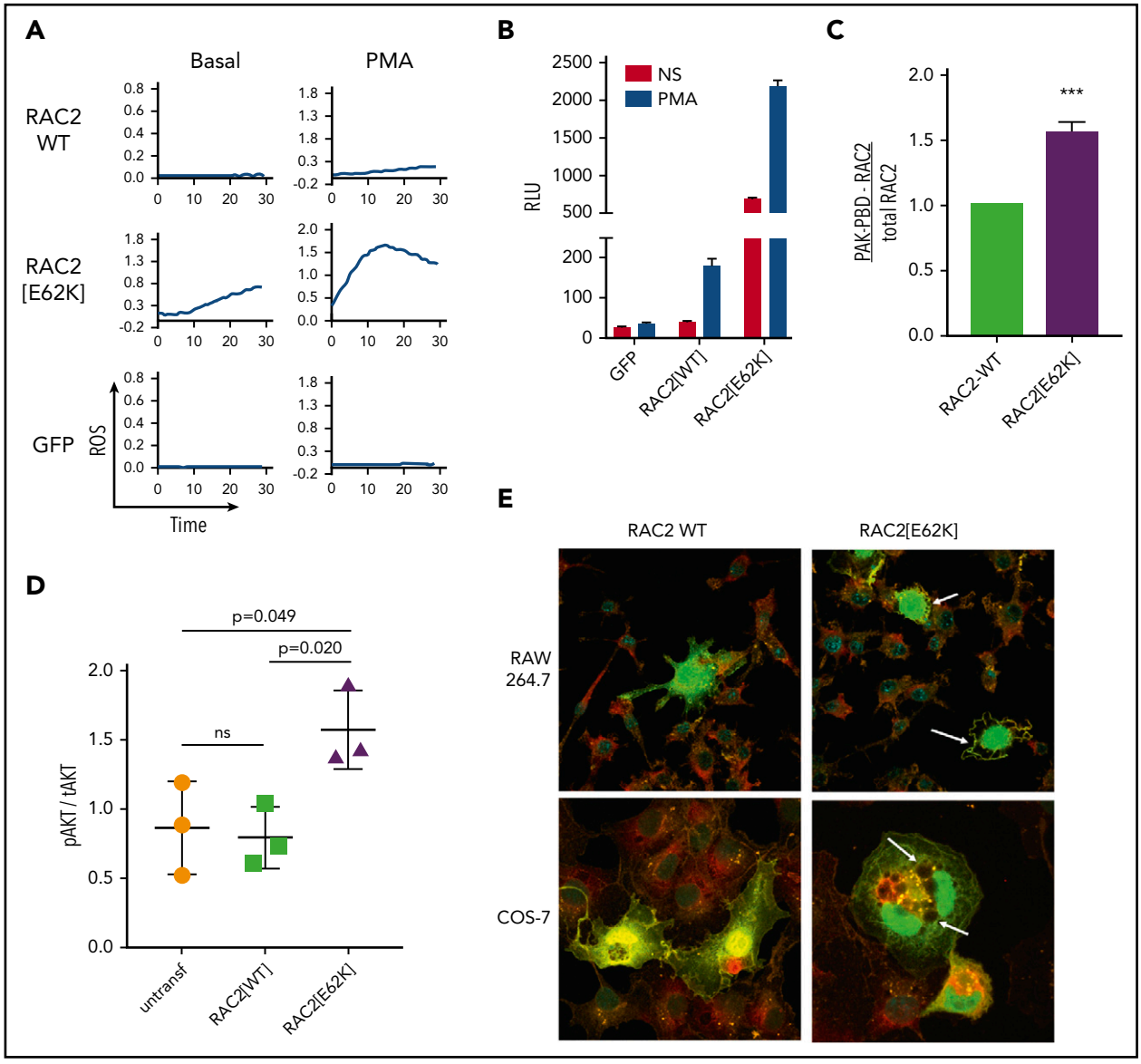

Figure 3. Transfection of RAC2[E62K] drives increased ROS production, increased RAC2[E62K] association with PAK-protein binding domain, increased pAKT, and increased membrane ruffling and macropinocytosis. (A) Diogenes assay to measure ROS production in COS-7 cells transfected with NADPH oxidase components (gp91^{phox}, p47^{phox}, p67^{phox}) and either RAC2[WT] (top), RAC2[E62K] (middle), or GFP (bottom) without stimulation (left) or after addition of 1 μM PMA (right). (B) Cumulative ROS production without (open bar) or with (filled bar) PMA stimulation; graph shows average ± standard error of the mean (SEM) of 1 representative experiment. (C) Immunoprecipitation of COS-7 cells transfected with RAC2[WT] or RAC2[E62K] using PAK1-PBD. Graph shows average ± SEM of 3 independent experiments. ***P = .0004. (D) Lysates from COS-7 cells transfected with RAC2[WT], RAC2[E62K], or untransfected were immunoblotted and stained for total AKT (tAKT) or phospho-AKT (S473). Bands were quantified by densitometry and the ratio of active, phospho-AKT/tAKT was plotted. Graph shows average ± SEM of 3 independent experiments (supplemental Figure 2B-D). (E) Confocal images of RAW264.7 cells (top, original magnification ×333) or COS-7 cells (bottom, original magnification ×235) transfected with RAC2[WT] (left) or RAC2[E62K] (right) and GFP as a transfection control. Cells were stained with Alexa-594-phalloidin (orange) to detect F-actin and Alexa-647-anti-RAC2 (red). Images were captured by a Zeiss LSM 880 confocal microscope and processed using the ZEN 2.3 lite program.

RAC2[WT] and RAC2[E62K] demonstrated similar intrinsic rates of GDP exchange (open circles, Figure 4A). However, in the presence of TIAM1, RAC2[WT] exchanged the majority of preloaded ^{mant}GDP (filled red circles), whereas RAC2[E62K] (filled blue circles) increased only slightly over the intrinsic rate. The calculated ^{mant}GDP dissociation rates from RAC2[WT] were significantly greater than RAC2[E62K], indicating impaired GDP release or exchange (Figure 4B).

We next examined intrinsic and p50RhoGAP-mediated GTP hydrolysis to determine whether p50RhoGAP enhanced RAC2 [E62K] GTP hydrolysis. As with GDP exchange, intrinsic rates of GTP hydrolysis were similar between RAC2[WT] and RAC2[E62K] proteins (Figure 4C). Unlike RAC2[WT] protein (filled red circles), the addition of p50RhoGAP failed to drive GTP hydrolysis of RAC2[E62K]. The addition of p50RhoGAP increased RAC2[WT] GTP hydrolysis sixfold, whereas RAC2[E62K] hydrolysis remained at the intrinsic rate despite the presence of p50RhoGAP (quantitated in Figure 4D). Taken together, these data show that RAC2[E62K] impairs GAP-mediated GTP hydrolysis, resulting in sustained GTP association and prolonged RAC2-driven activation of downstream effectors.

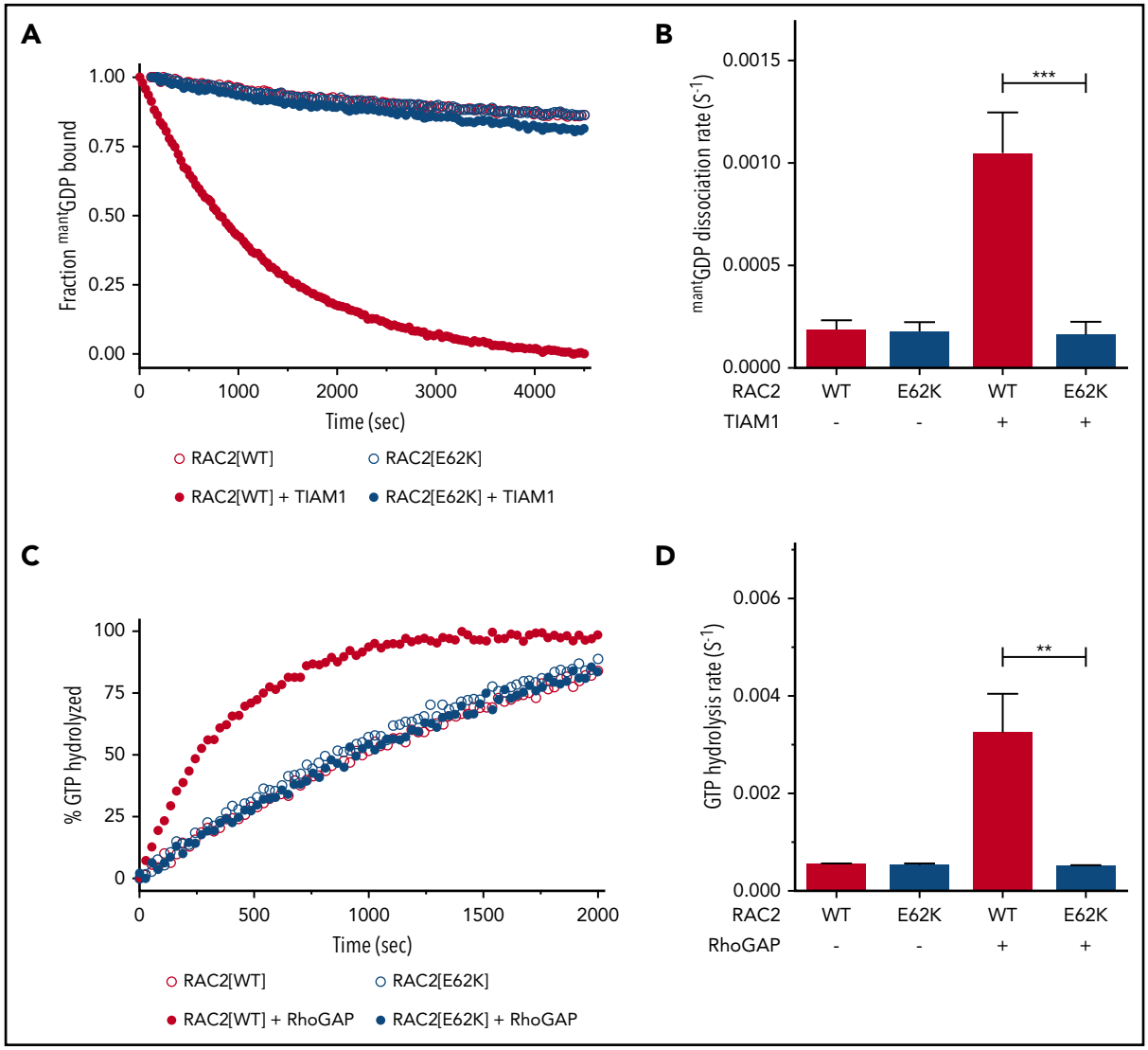

Figure 4. RAC2[E62K] has altered TIAM1-mediated GDP exchange and p50RhoGAP-mediated GTP hydrolysis. (A) GDP exchange assay using RAC2[WT] (red) and RAC2 [E62K] (blue) preloaded with fluorescent ^{mant}GDP and incubated with unlabeled GDP. Intrinsic nucleotide exchange (open circles) and TIAM1-mediated exchange (filled circles) are shown. Ratio TIAM1:RAC2 = 1:1. (B) ^{mant}GDP dissociation rate of RAC2[WT] and RAC2[E62K] with and without TIAM1 calculated from panel A. Number of replicates, N = 4 for intrinsic dissociation and N = 2 for TIAM1-mediated dissociation. ***$P < .0005$. (P value calculated using the 1-way ANOVA followed by Tukey multiple comparison test). (C) GTP hydrolysis of RAC2[WT] and RAC2[E62K] preloaded with GTP without and with p50RhoGAP (1:500, p50RhoGAP:RAC2). Colored as in panel A. (D) GTP hydrolysis rate of RAC2[WT] and RAC2[E62K] preloaded with GTP, calculated from panel C. Data acquired in triplicate. **$P < .005$ (P value calculated as in panel B).

Rac2$^{+/E62K}$ mice have lymphopenia and excess neutrophil $O_2^{\cdot-}$ production

To further evaluate the effects of RAC2[E62K] in lymphoid and myeloid cells in vivo, we generated Rac2$^{+/E62K}$ mice by using CRISPR/cas9 to introduce Rac2[E62K] into C57BL6 mouse embryos.

All RAC2[E62K] patients identified to date had T- and B-cell lymphopenia (Table 1); 2 patients, 1 reported here and 1 RAC2 [D57N] patient, both identified through newborn screening,[29] had reduced newborn TRECs. We used peripheral blood from 8- to 10-week-old Rac2$^{+/+}$ and Rac2$^{+/E62K}$ mice to analyze lymphocyte subsets. Rac2$^{+/E62K}$ mice had profoundly decreased circulating lymphocytes compared with Rac2$^{+/+}$(Figure 5A). There was a >20-fold decrease in CD3$^+$ T cells, reflecting decreases of both CD4$^+$ and CD8$^+$ cells. The Rac2$^{+/E62K}$ B-cell compartment was reduced, with fewer NK1.1$^+$ cells (supplemental Figure 3A) in the Rac2$^{+/E62K}$ mice, although the differences did not reach statistical significance.

To further explore the peripheral lymphopenia, splenic lymphocyte subsets from 18-week-old mice were examined. Although total cellularity was not different between the Rac2$^{+/E62K}$ and Rac2$^{+/+}$ spleens (supplemental Figure 3B), there was a profound increase in Mac1$^+$ cells (Figure 5B) with high side scatter, consistent with neutrophilia. Splenic B cells were not significantly decreased; however, T-cell receptor αβ$^+$ (TCRαβ$^+$) cells were lower in Rac2$^{+/E62K}$ mice even though TCRγδ$^+$ cell numbers were preserved (Figure 5B). Both single positive T-cell subsets were decreased, with CD8$^+$ T cells exhibiting a larger decrease than CD4$^+$ T cells (Figure 5C). Given the profound lymphopenia, we examined thymic T-cell subsets. Similar to the spleen, total cellularity was equivalent. Percentages of double-negative (DN), double-positive,

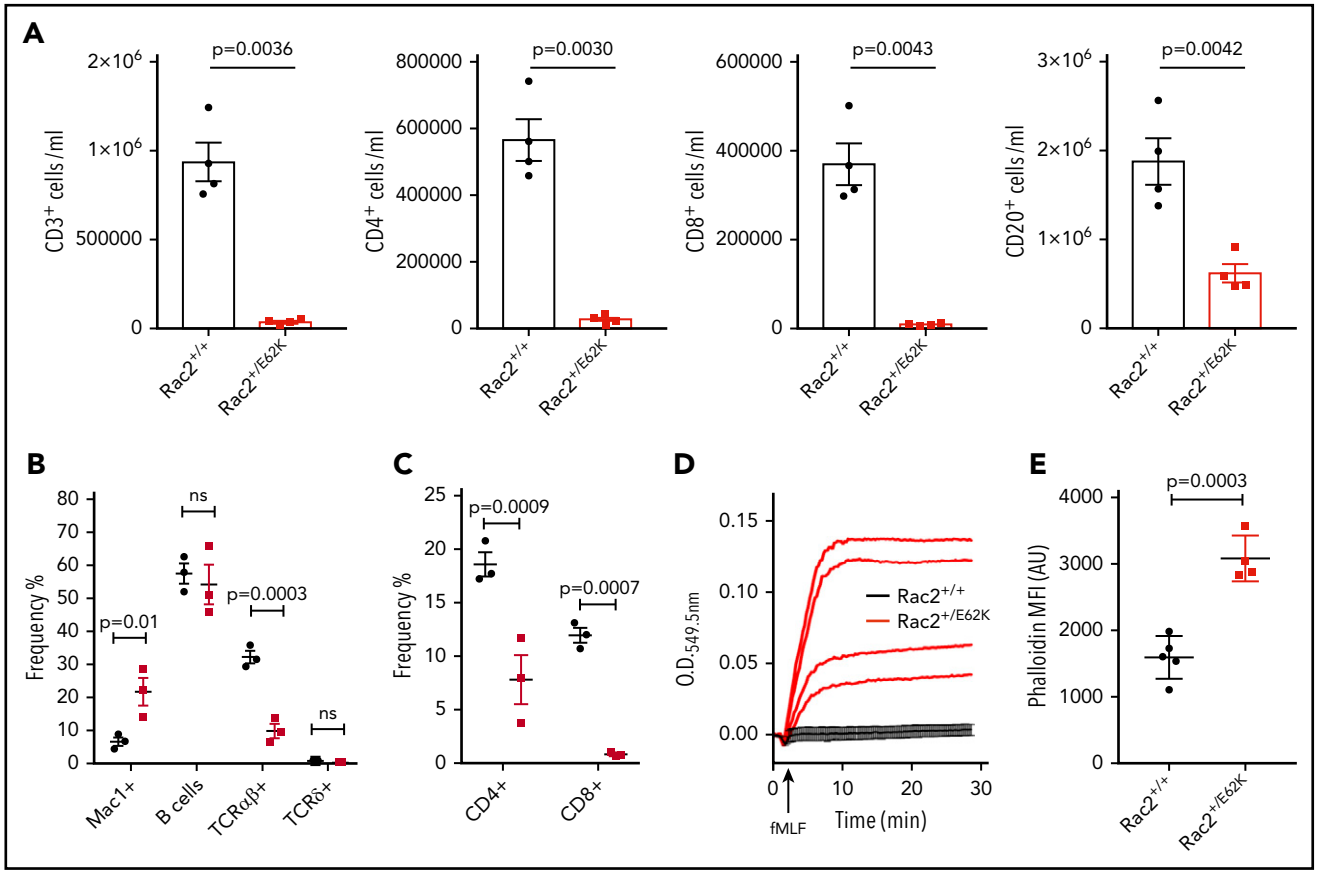

Figure 5. Rac2$^{+/E62K}$ mice recapitulate cytopenias, superoxide production, and increased neutrophil F-actin content seen in patients. (A) Peripheral blood cells from Rac2$^{+/+}$ and Rac2$^{+/E62K}$ mice stained for lineage markers (n = 4 each group). Top, from left: CD3$^+$ T cells, CD3$^+$CD4$^+$ T cells, CD3$^+$CD8$^+$ T cells, and CD20$^+$ B cells (*P* value calculated using Student *t* test with Welch correction). (B) Splenic cell populations from Rac2$^{+/+}$ and Rac2$^{+/E62K}$ mice identified by noted markers. Two-way ANOVA with Sidak multiple comparison test was used to determine significance. (C) Splenic T-cell subsets from Rac2$^{+/+}$ and Rac2$^{+/E62K}$ mice identified by noted markers. Two-way ANOVA with Sidak multiple comparison test was used to determine significance. (D) Superoxide production after addition of fMLF in bone marrow neutrophils from Rac2$^{+/+}$ (black lines) and Rac2$^{+/E62K}$ mice (red lines). Results combined from 2 independent experiments. (E) Phalloidin staining for F-actin in mouse bone marrow neutrophils from Rac2$^{+/+}$ and Rac2$^{+/E62K}$ mice (n = 4 each group). Results combined from 2 independent experiments.

and CD4$^+$ and CD8$^+$ single-positive cells were also similar between the 2 groups (supplemental Figure 3C). Gross thymic size indicated that traffic from the bone marrow was not limiting and so did not explain the peripheral lymphopenia. Similarly, maturation from DN, through double positive to single positive cells appeared intact in the Rac2$^{+/E62K}$ mice, indicating that the lymphopenia did not arise during thymic maturation.

Given the neutrophil defects seen in patient cells, we examined fMLF-induced $O_2^{\bullet-}$ production and F-actin content in bone marrow neutrophils. Similar to patients, we observed increased $O_2^{\bullet-}$ production in response to fMLF in Rac2$^{+/E62K}$ compared with Rac2$^{+/+}$ mouse marrow cells (Figure 5D). Likewise, bone marrow neutrophils from Rac2$^{+/E62K}$ mice exhibit elevated F-actin as demonstrated by increased phalloidin staining (Figure 5E). Therefore, Rac2$^{+/E62K}$ mice recapitulate the lymphocyte and neutrophil defects identified in 3 patients with the RAC2[E62K] mutation.

Discussion

We identified de novo RAC2 p.E62K in 3 unrelated patients, 2 of whom had recurrent upper respiratory infections and immunodeficiency, whereas the third was detected by newborn screening. Unlike the previously reported RAC2 loss-of-function mutation, p.D57N, or the homozygous null p.W56X mutation, RAC2[E62K] is a gain-of-function mutation that prevents hydrolysis of the GTP nucleotide, resulting in prolonged activation of downstream effectors, such as p67^{phox} and PAK1.

RAC2[E62K] is an activating mutation

Increases in $O_2^{\bullet-}$ production, macropinocytosis, membrane ruffling, and altered cellular migration in patient and transfected cells are most consistent with RAC2[E62K] being an activating mutation. This is consonant with other activating Switch II mutations in the RAC family, RAC2[Q61L],[30] RAC2[D63V],[22] and CDC42 [Y64C],[23] which impair GDP exchange and GTP hydrolysis. Notably, the crystal structure of Rac1 bound to the GAP domain of *Salmonella sptP* identifies the 4 conserved amino acids, Q61, E62, D63, and Y64, in direct contact with the GAP protein domain,[31] suggesting that mutations at these amino acids could inhibit GAP binding to the activated Rac molecule leading to extended RAC activation. Somatic, activating RAS family mutations, including those of Q61, are the most common driver mutations in multiple malignancies (Catalogue of Somatic Mutations in Cancer database [COSMIC], https://cancer.sanger.ac.uk), occurring in 27% of all human cancers.[32] Pharmacologic efforts to target these activating mutations with small molecule inhibitors rely on mutation-positive

cancer-derived cell lines. The Rac2$^{+/E62K}$ mouse could provide a model for testing these inhibitors in the setting of germline rather than somatic mutation. These related Switch II mutations with similar biochemical features, both germline and somatic, underscore the dominant effect caused by prolonged activation of RAC2[E62K].

RAC2 binds to effector proteins p67^{phox} and PAK1

Studies in mouse Rac2$^{-/-}$ neutrophils have demonstrated different effector proteins involved in $O_2^{\bullet}$ production (p67^{phox}) and cell migration (Pak1), indicating that multiple pathways are affected by the loss of Rac2 in these cells.[26,33,34] The ability of RAC2 to cycle between GDP- and GTP-bound forms allows it to act as a molecular switch because only active RAC2-GTP can bind to p67^{phox35} or PAK1.[12] Activation of PAK1 after stimulation leads to its relocation to areas of active cytoskeletal rearrangement,[36] while transfection of a mutant, activated PAK1 induces membrane ruffles and accumulation of F-actin.[2] Ex vivo studies using patient neutrophils demonstrated prolonged production of $O_2^{\bullet}$, suggesting an extended p67^{phox}-RAC2-GTP association. Likewise, we found increased RAC2[E62K]-PAK1 association in RAC2[E62K]-transfected cells, indicating an increased proportion of RAC2[E62K] in the active GTP-bound state compared with RAC2[WT].

Activated RAC2[E62K] impairs actin remodeling

Inactivation of RAC is required for F-actin disassembly and phagocytic cup closure.[36] Using cells transfected with a photoactivated RAC1, Fujii et al[24] produced membrane ruffling and unclosed premacropinosomes when the cells were activated by exposure to blue light. When the light was turned off, inactivating RAC1, the ruffling ceased and the macropinosomes closed and acquired maturation markers, demonstrating the requirements of RAC-GTP/GDP cycling for completion of the process. Impaired GAP-mediated RAC2[E62K]-GTP hydrolysis maintains the active state and interferes with on/off cycling. Accumulation of F-actin in patient and mouse cells and membrane ruffling in transfected RAW264.7 cells is consistent with prolonged activation of this RAC2 mutant. In contrast to RAC2[E62K]-transfected cells, the dominant loss-of-function RAC2[D57N] inhibited membrane ruffling and macropinosome formation in primary murine bone marrow–derived macrophages.[3] Likewise, elevated F-actin seen in patient cells indicates a breakdown in actin cycling within RAC2[E62K] neutrophils. Decreased cycling between F-actin and G-actin is expected to result in impaired chemotaxis and macropinosome closure, both of which we observed in patient neutrophils.

Effects of RAC2 mutations on lymphocyte development

All RAC2 patients so far identified have exhibited profound lymphopenia. The resolution of lymphopenia posthematopoietic stem cell transplant in patient 1 indicates this is a hematopoietic cell intrinsic defect and not caused by a functional defect in thymic epithelial cells. In Rac2$^{-/-}$ mice, T-cell development occurs normally, most likely from functional redundancy between Rac1 and Rac2.[37] This is apparent in Rac2$^{-/-}$ Rac1$^{flox/flox}$ mice crossed with CD2- or CD19-driven Cre recombinase mice lacking both Rac1 and Rac2 in their T[38] or B cells,[39] respectively. Loss of both Rac1 and Rac2 in mouse T cells resulted in decreased total thymocyte number and altered T-cell maturation from DN through single positive. In Rac1/Rac2-deficient CD19 cells, bone marrow B-cell development appeared preserved across genotypes. However, Rac1/Rac2-deficient mice exhibited drastically reduced splenic and circulating mature B cells. These 2 studies provide evidence for the requirement of Rac2 during T- and B-cell maturation.

Although RAC2[E62K] patients and Rac2$^{+/E62K}$ mice exhibit both T- and B-cell lymphopenia, thymic cellularity in the Rac2$^{+/E62K}$ mice provides evidence the T lymphopenia is not the result of bone marrow emigration into the thymus. Likewise, T-cell maturation within the thymus appears to be maintained. Several mutations affecting actin remodeling have been implicated in T-cell lymphopenia, including cofilin (*Cfl1*),[40] coronin 1a (*CORO1A*),[41] *Dock8*,[42] WASp (*WAS*),[43] and *ARPC1B*,[44] each affecting thymocyte development differently. Nonfunctional cofilin leads to a developmental arrest during DN2 to DN3 stage of thymocyte maturation resulting from failure of TCRβ surface expression.[40] Different mutations within *Coro1a* cause lymphopenia by different mechanisms; T cells from *Ptcd* mice have impaired thymic egress, whereas Koy mice, with unstable Coro1a protein, have reduced thymocyte survival.[40] Dock8$^{cpm/cpm}$ mice have thymic accumulation of CD4$^+$ cells and decreased survival of both CD4$^+$ and CD8$^+$ cells.[45] Recently, decreased TRECs in patients and mice with *WAS* mutations were demonstrated along with decreased F-actin in patient T cells,[43] emphasizing the critical role of actin remodeling throughout thymic development and output. Additional experiments such as synchronized intrathymic injections of thymocytes to establish timing and location of T-cell loss or microscopy of thymic sections to examine individual cell trafficking may help elucidate the mechanism of Rac2$^{+/E62K}$ lymphopenia.

The majority of RAC2 studies have focused on analysis of Rac2$^{-/-}$ mice, inferring the function of Rac2. The patient genotypes now identified, dominant RAC2[D57N] loss of function, recessive RAC2[W57X] null, and dominant RAC2[E62K] gain of function, as well as the Rac2$^{+/E62K}$ mouse clarify distinct roles of RAC2 in hematopoiesis and actin cytoskeleton remodeling in immune cells. These data also support the inclusion of *RAC2* on primary immune deficiency sequencing panels for patients with low/absent TRECs, T-cell lymphopenia, or CVID.

Acknowledgments

The authors thank the patients and their families for participating in this study, Javier Manzella-Lapeira (National Institute of Allergy and Infectious Diseases [NIAID]) for help in confocal microscopy and image analysis, the Mouse Genetics and Gene Modification Core (NIAID) for assistance producing the Rac2$^{+/E62K}$ mouse, Ryan Kissinger (NIAID) for assistance with the graphical abstract, and Michael Lenardo (NIAID) for critical reading of the manuscript.

This project was supported in part by grants from the National Institutes of Health Intramural Research Program, NIAID, and the National Cancer Institute (HHSN261200800001E and P01 CA203657) (S.L.C.).

The content of this publication does not necessarily reflect the views or policies of the Department of Health and Human Services, nor does mention of trade names, commercial products, or organizations imply endorsement by the US Government.

Authorship

Contribution: A.P.H., T.L.L., S.C., M.S.L., and D.B.K. conceived and designed experiments; A.P.H., A. Donkó, M.E.A., M.S., D.F., A. Das, and O.E. performed the experiments; A.P.H., A. Donkó, M.E.A., M.S., D.F., A. Das, A.B., and D.B.K. analyzed the data; V.B., P.S., H.N.S., J.B., A.S., M.M., J.D., C.P., L.F., R.L.F., J.A.C., and S.M.H. provided clinical care;

A.B., T.L.L., S.C., M.S.L., D.B.K., and S.M.H. provided reagents, materials, and analysis tools; A.P.H., S.M.H., and M.S.L. wrote the manuscript; and all authors read and approved the final manuscript.

Conflict-of-interest disclosure: The authors declare no competing financial interests.

ORCID profiles: A.P.H., 0000-0001-6841-2122; S.C., 0000-0003-0311-409X.

Correspondence: Amy P. Hsu, National Institutes of Health, Building 10, Room 11S257, 9000 Rockville Pike, Bethesda, MD 20892; e-mail: amy.hsu@nih.gov.

Footnotes

Submitted 14 November 2018; accepted 29 January 2019. Prepublished online as *Blood* First Edition paper, 5 February 2019; DOI 10.1182/blood-2018-11-886028.

*A. Donkó, M.E.A., M.S., and D.F. contributed equally to this work.

The online version of this article contains a data supplement.

The publication costs of this article were defrayed in part by page charge payment. Therefore, and solely to indicate this fact, this article is hereby marked "advertisement" in accordance with 18 USC section 1734.

REFERENCES

1. Knaus UG, Heyworth PG, Evans T, Curnutte JT, Bokoch GM. Regulation of phagocyte oxygen radical production by the GTP-binding protein Rac 2. *Science*. 1991; 254(5037):1512-1515.
2. Sells MA, Knaus UG, Bagrodia S, Ambrose DM, Bokoch GM, Chernoff J. Human p21-activated kinase (Pak1) regulates actin organization in mammalian cells. *Curr Biol*. 1997;7(3):202-210.
3. Abell AN, DeCathelineau AM, Weed SA, Ambruso DR, Riches DW, Johnson GL. Rac2D57N, a dominant inhibitory Rac2 mutant that inhibits p38 kinase signaling and prevents surface ruffling in bone-marrow-derived macrophages. *J Cell Sci*. 2004;117(Pt 2): 243-255.
4. Hoppe AD, Swanson JA. Cdc42, Rac1, and Rac2 display distinct patterns of activation during phagocytosis. *Mol Biol Cell*. 2004; 15(8):3509-3519.
5. Ambruso DR, Knall C, Abell AN, et al. Human neutrophil immunodeficiency syndrome is associated with an inhibitory Rac2 mutation. *Proc Natl Acad Sci USA*. 2000;97(9): 4654-4659.
6. Accetta D, Syverson G, Bonacci B, et al. Human phagocyte defect caused by a Rac2 mutation detected by means of neonatal screening for T-cell lymphopenia. *J Allergy Clin Immunol*. 2011;127(2):535-538.e1, 2.
7. Alkhairy OK, Rezaei N, Graham RR, et al. RAC2 loss-of-function mutation in 2 siblings with characteristics of common variable immunodeficiency. *J Allergy Clin Immunol*. 2015; 135(5):1380-4.e1, 5.
8. Li S, Yamauchi A, Marchal CC, Molitoris JK, Quilliam LA, Dinauer MC. Chemoattractant-stimulated Rac activation in wild-type and Rac2-deficient murine neutrophils: preferential activation of Rac2 and Rac2 gene dosage effect on neutrophil functions. *J Immunol*. 2002;169(9):5043-5051.
9. Kim C, Dinauer MC. Rac2 is an essential regulator of neutrophil nicotinamide adenine dinucleotide phosphate oxidase activation in response to specific signaling pathways. *J Immunol*. 2001;166(2):1223-1232.
10. Haeusler LC, Blumenstein L, Stege P, Dvorsky R, Ahmadian MR. Comparative functional analysis of the Rac GTPases. *FEBS Lett*. 2003; 555(3):556-560.
11. Nisimoto Y, Freeman JL, Motalebi SA, Hirshberg M, Lambeth JD. Rac binding to p67 (phox). Structural basis for interactions of the Rac1 effector region and insert region with components of the respiratory burst oxidase. *J Biol Chem*. 1997;272(30):18834-18841.
12. Knaus UG, Wang Y, Reilly AM, Warnock D, Jackson JH. Structural requirements for PAK activation by Rac GTPases. *J Biol Chem*. 1998; 273(34):21512-21518.
13. Lorès P, Morin L, Luna R, Gacon G. Enhanced apoptosis in the thymus of transgenic mice expressing constitutively activated forms of human Rac2GTPase. *Oncogene*. 1997;15(5): 601-605.
14. Zhang S, Han J, Sells MA, et al. Rho family GTPases regulate p38 mitogen-activated protein kinase through the downstream mediator Pak1. *J Biol Chem*. 1995;270(41): 23934-23936.
15. Jennings RT, Knaus UG. Rho family and Rap GTPase activation assays. *Methods Mol Biol*. 2014;1124:79-88.
16. Hobbs GA, Mitchell LE, Arrington ME, et al. Redox regulation of Rac1 by thiol oxidation. *Free Radic Biol Med*. 2015;79:237-250.
17. Yin G, Kistler S, George SD, et al. A KRAS GTPase K104Q mutant retains downstream signaling by offsetting defects in regulation. *J Biol Chem*. 2017;292(11):4446-4456.
18. Lionakis MS, Lim JK, Lee CC, Murphy PM. Organ-specific innate immune responses in a mouse model of invasive candidiasis. *J Innate Immun*. 2011;3(2):180-199.
19. Swamydas M, Lionakis MS. Isolation, purification and labeling of mouse bone marrow neutrophils for functional studies and adoptive transfer experiments. *J Vis Exp*. 2013; (77): e50586.
20. Gasper R, Thomas C, Ahmadian MR, Wittinghofer A. The role of the conserved switch II glutamate in guanine nucleotide exchange factor-mediated nucleotide exchange of GTP-binding proteins. *J Mol Biol*. 2008;379(1):51-63.
21. Zehir A, Benayed R, Shah RH, et al. Mutational landscape of metastatic cancer revealed from prospective clinical sequencing of 10,000 patients. *Nat Med*. 2017;23(6):703-713.
22. Caye A, Strullu M, Guidez F, et al. Juvenile myelomonocytic leukemia displays mutations in components of the RAS pathway and the PRC2 network. *Nat Genet*. 2015;47(11): 1334-1340.
23. Martinelli S, Krumbach OHF, Pantaleoni F, et al; University of Washington Center for Mendelian Genomics. Functional dysregulation of CDC42 causes diverse developmental phenotypes. *Am J Hum Genet*. 2018;102(2): 309-320.
24. Fujii M, Kawai K, Egami Y, Araki N. Dissecting the roles of Rac1 activation and deactivation in macropinocytosis using microscopic photomanipulation. *Sci Rep*. 2013;3(1):2385.
25. Williams DA, Tao W, Yang F, et al. Dominant negative mutation of the hematopoietic-specific Rho GTPase, Rac2, is associated with a human phagocyte immunodeficiency. *Blood*. 2000;96(5):1646-1654.
26. Roberts AW, Kim C, Zhen L, et al. Deficiency of the hematopoietic cell-specific Rho family GTPase Rac2 is characterized by abnormalities in neutrophil function and host defense. *Immunity*. 1999;10(2):183-196.
27. Sun CX, Magalhães MAO, Glogauer M. Rac1 and Rac2 differentially regulate actin free barbed end formation downstream of the fMLP receptor. *J Cell Biol*. 2007;179(2): 239-245.
28. Higuchi M, Onishi K, Kikuchi C, Gotoh Y. Scaffolding function of PAK in the PDK1-Akt pathway. *Nat Cell Biol*. 2008;10(11): 1356-1364.
29. Routes JM, Grossman WJ, Verbsky J, et al. Statewide newborn screening for severe T-cell lymphopenia. *JAMA*. 2009;302(22): 2465-2470.
30. Xu X, Wang Y, Barry DC, Chanock SJ, Bokoch GM. Guanine nucleotide binding properties of Rac2 mutant proteins and analysis of the responsiveness to guanine nucleotide dissociation stimulator. *Biochemistry*. 1997;36(3): 626-632.
31. Stebbins CE, Galán JE. Modulation of host signaling by a bacterial mimic: structure of the Salmonella effector SptP bound to Rac1. *Mol Cell*. 2000;6(6):1449-1460.
32. Hobbs GA, Der CJ, Rossman KL. RAS isoforms and mutations in cancer at a glance. *J Cell Sci*. 2016;129(7):1287-1292.
33. Gu Y, Williams DA. RAC2 GTPase deficiency and myeloid cell dysfunction in human and mouse. *J Pediatr Hematol Oncol*. 2002;24(9): 791-794.
34. Carstanjen D, Yamauchi A, Koornneef A, et al. Rac2 regulates neutrophil chemotaxis, superoxide production, and myeloid colony formation through multiple distinct effector pathways. *J Immunol*. 2005;174(8): 4613-4620.

35. Koga H, Terasawa H, Nunoi H, Takeshige K, Inagaki F, Sumimoto H. Tetratricopeptide repeat (TPR) motifs of p67(phox) participate in interaction with the small GTPase Rac and activation of the phagocyte NADPH oxidase. *J Biol Chem*. 1999;274(35): 25051-25060.

36. Schlam D, Bagshaw RD, Freeman SA, et al. Phosphoinositide 3-kinase enables phagocytosis of large particles by terminating actin assembly through Rac/Cdc42 GTPase-activating proteins. *Nat Commun*. 2015;6(1): 8623.

37. Troeger A, Williams DA. Hematopoietic-specific Rho GTPases Rac2 and RhoH and human blood disorders. *Exp Cell Res*. 2013; 319(15):2375-2383.

38. Dumont C, Corsoni-Tadrzak A, Ruf S, et al. Rac GTPases play critical roles in early T-cell development. *Blood*. 2009;113(17):3990-3998.

39. Walmsley MJ, Ooi SK, Reynolds LF, et al. Critical roles for Rac1 and Rac2 GTPases in B cell development and signaling. *Science*. 2003;302(5644):459-462.

40. Seeland I, Xiong Y, Orlik C, et al. The actin remodeling protein cofilin is crucial for thymic αβ but not γδ T-cell development. *PLoS Biol*. 2018;16(7):e2005380.

41. Shiow LR, Roadcap DW, Paris K, et al. The actin regulator coronin 1A is mutant in a thymic egress-deficient mouse strain and in a patient with severe combined immunodeficiency. *Nat Immunol*. 2008;9(11): 1307-1315.

42. Dasouki M, Okonkwo KC, Ray A, et al. Deficient T cell receptor excision circles (TRECs) in autosomal recessive hyper IgE syndrome caused by DOCK8 mutation: implications for pathogenesis and potential detection by newborn screening. *Clin Immunol*. 2011;141(2):128-132.

43. Li W, Sun X, Wang J, et al. Defective thymic output in WAS patients is associated with abnormal actin organization. *Sci Rep*. 2017; 7(1):11978.

44. Brigida I, Zoccolillo M, Cicalese MP, et al. T-cell defects in patients with *ARPC1B* germline mutations account for combined immunodeficiency. *Blood*. 2018;132(22):2362-2374.

45. Lambe T, Crawford G, Johnson AL, et al. DOCK8 is essential for T-cell survival and the maintenance of CD8+ T-cell memory. *Eur J Immunol*. 2011;41(12): 3423-3435.

46. Krauthammer M, Kong Y, Ha BH, et al. Exome sequencing identifies recurrent somatic RAC1 mutations in melanoma. *Nat Genet*. 2012; 44(9):1006-1014.